Austrian Journal of Earth Sciences | Volume 103/2 | 81 - 91 | Vienna | 2010

Quaternary celestine and gypsum extensional veins in a folded hypersaline lake infill: the Qaidam basin, western China

Franz NEUBAUER[1)*)], Yongjiang LIU[2)], Johann GENSER[1)], Andrea Brigitte RIESER[1)3)], Gertrude FRIEDL[1)], Xiaohong GE[2)] & Martin THÖNI[4)]

[1)] Dept. Geography and Geology, University of Salzburg, Hellbrunnerstr. 34, A-5020 Salzburg, Austria;

[2)] Faculty of Earth Sciences, Jilin University, 130061 Changchun, China;

[3)] present address: Nagra, Hardstrasse 73, 5430 Wettingen, Switzerland;

[4)] Dept. of Lithospheric Research, Vienna University, Althanstr. 14, A-1090 Vienna, Austria;

[*)] Corresponding author, franz.neubauer@sbg.ac.at

KEYWORDS

Sr isotopic stratigraphy
extensional vein
Qaidam basin
celestine
brine

Abstract

The nonmarine, at present hypersaline Qaidam basin of Western China comprises a ca. 8–17 km thick sedimentary fill, which is dominated by Eocene to Recent clastic rocks. These successions were folded due to ongoing India-Eurasia convergence from late Miocene onwards until today. Shortening also resulted in enhanced fluid flow and precipitation of sulphate minerals in subvertical tension gashes, which are mainly filled by celestine and fibrous gypsum. The orientation of subvertical veins is similar over most parts of the western Qaidam basin and indicates NNE-SSW to N-S shortening (present-day coordinates) dissimilar to the NE-motion direction deduced from recent geodetic (GPS) data. In deeper stratigraphic levels of anticlinal cores, tension gashes composed of fibrous gypsum subparallel to bedding demonstrate fluid overpressure during their formation at a shallow structural level, below the conversion temperature of gypsum to anhydrite. We interpret all these veins as near-surface precipitates from sulphate-rich brines during an advanced stage of folding. The $^{87}Sr/^{86}Sr$ ratios of a synsedimentary celestine layer and a celestine vein at the abandoned Dafengshan mine are 0.711414 and 0.711418, respectively, and are similar to those from Oligocene and Miocene limestones (0.711578 to 0.711679). Although the source area is highly heterogeneous in composition, these data indicate, therefore, in accordance with previous observations on clastic rocks, only a very minor change in the average $^{87}Sr/^{86}Sr$ ratio of the source region from Oligocene to Quaternary times.

Das nichtmarine, heute hypersalinare Qaidam-Becken in Westchina ist mit 8 – 17 km mächtigen eozänen bis rezenten, vorwiegend klastischen Sedimenten gefüllt, die, bedingt durch die Konvergenz zwischen Indien und Eurasien, vom späten Miozän bis heute verfaltet wurden. Die Verkürzung führt auch zu einem verstärkten Fluidfluss und Fällung von Sulfaten in subvertikalen Dehnungsklüften, die hauptsächlich mit Cölestin und fibrösem Gips gefüllt sind. Die Orientierung der subvertikalen Adern ist über weite Teile des westlichen Qaidam-Beckens ähnlich und zeigt NNE-SSW bis N-S-Verkürzung (in heutigen Koordinaten) an. Diese Orientierung weicht von der heutigen Nordostbewegung der rezenten geodätischen Daten (GPS) ab. In tieferen stratigraphischen Niveaus von Antiklinalkernen zeigen schichtparallele Adern aus fibrösem Gips Fluidüberdruck während deren Bildung an, und zwar unterhalb der Umwandlungstemperatur von Gips zu Anhydrit. Wir interpretieren alle Typen dieser sulfatischen Gänge als erdoberflächennahe Fällungen aus sulfatreichen Solen während eines fortgeschrittenen Stadiums der Faltung. Die $^{87}Sr/^{86}Sr$-Verhältnisse von synsedimentären Cölestinlagen und von Cölestinadern liegen bei 0.711414 und 0.711418. Diese sind ähnlich zu solchen von oligozänen und miozänen Kalken (0.711578 to 0.711679). Obwohl das Hinterland heterogen zusammengesetzt ist, zeigen diese $^{87}Sr/^{86}Sr$-Verhältnisse, ähnlich zu Beobachtungen in klastischen Sedimenten, nur geringe Änderungen des Liefergebiets seit dem Oligozän an.

1. Introduction

Tension gashes (or extensional veins) filled by a variety of minerals including quartz and calcite are common in many metamorphic successions, particularly in such of very low-grade metamorphic terrains (e.g., Ramsay and Huber, 1983; Groshong, 1988; Bons, 2000, 2001; Hausegger et al., 2009; Holland and Urai, 2009). Such tension gashes are commonly interpreted to result from precipitation from subsurface fluids, which are sometimes under overpressure (e.g., Gudmundsson et al., 2001; Philipp, 2008). The fluid overpressure of hydrofractures is defined as the fluid pressure exceeding the normal pressure to the fracture (mode I cracks), which for extensional fractures is the minimum principal compressive stress σ_3 (Gudmundsson et al., 2001). Veins are also commonly formed by hydrothermal fluids invading country rocks in a late stage of their evolution (Craw and Campbell, 2004 and references therein), and these veins reflect the regional stress conditions during their formation (e.g., Sibson, 2001, 2003; Neubauer et al., 2005). Gypsum-filled veins have been reported only from a few locations (Warrak, 1996; Philipp, 2008). However, to our knowledge, no reports exist on celestine veins.

In this contribution, we document an unusual composition of sulphatic veins from the Qaidam basin at the northern margin of the Tibet plateau, particularly of celestine and gypsum veins and discuss their origin in respect to the overall hydrological regime of the basin fill. Furthermore, we use these veins to constrain the overall shortening direction of the Qai-

dam basin during Quaternary and compare these results with those of recent geodetic measurements. We also use the Sr isotopic composition of the celestine veins in conjunction with that of Oligocene and Miocene limestones to show possible variations. We found no significant change between Oligocene and Quaternary. This is interesting in terms of the quite heterogeneous composition of the source in adjacent mountain belts and argues that no significant change of the hinterland occurred since Oligocene, at least as far as Sr isotopes are concerned. Description and interpretation of sulphate veins are based on work of Hanor (2000) and Spencer (2000).

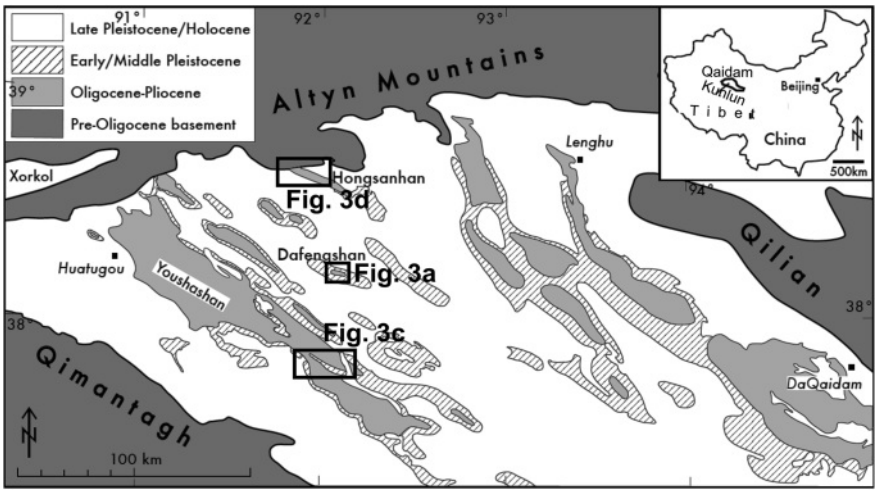

Figure 1: Location of the Qaidam basin in northwestern China, at the northeastern corner of the Tibetan plateau. Note the endorheic drainage pattern and the Altyn Mountains to the N and Kunlun/Qimantagh Mountains to the S of the basin. Note anticlines exposing Oligocene to Neogene successions. Map modified from Rieser et al. (2009).

2. GEOLOGICAL SETTING

The nonmarine, hypersaline Qaidam basin of Western China (Fig. 1) comprises a ca. 8–17 km thick sedimentary infill of Eocene to Recent mainly clastic rocks (Figs. 1, 2; Huang et al., 1997; Xia et al., 2001). Because of almost entirely endorheic drainage (Fig. 1), the infilling history is governed by erosion of surrounding mountain belts (Altyn, Kunlun, Qilian Mts.), climate and tectonic evolution (Rieser et al., 2006; Yin et al., 2008).

In general, the Qaidam basin represented a single, large lake over most of its lifetime (Huang et al., 1997; Wang et al., 1999). Alluvial deposits with coarse clastic sediments dominated the basin margin. Shore and deltaic deposits, mostly in the western Qaidam basin, are characterized by sandstones and the lake center facies comprises mainly mudstones and marls. A carbonate content of up to 30 percent is estimated for marls of the lake floor facies (e.g., Huang et al., 1997). The basin fill comprises a number of formations based on the occurrence of conglomerates at the base of some formations and seismic reflectors, which are constrained by borehole data. These formations and their chronostratigraphic assignments are shown in Fig. 2. The chronostratigraphy of these formations is based on limnic fossils such as ostracods and on palynology, magnetostratigraphy (e.g., Sun et al., 2005) and correlation with nearby basins like the Tarim basin and is discussed in length by Rieser et al. (2009). During the late Miocene, folding and shortening of the Qaidam basin fill started and the basin was progressively fragmented in anticlines, which separated individual smaller lakes (Zhou et al., 2006). These depressions were filled mainly by mudstones and marls. A trend of increasing aridity since Pliocene has been observed throughout the basin (e. g., Lowenstein et al., 1989; Schubel et al., 1991; Bojar et al., 2005; Tan et al., 2009). Superimposed on this trend, cyclic hypersaline stages during lake level lowstands and stages with a higher lake level have been documented (e.g., Philipps et al., 1993 and references therein), mostly for the Pleistocene (Qigequan Fm.). Based on U/Th dating, Philipps et al. (1993) reported three stages of low lake

Time (MA)	Epoch	Formation	
	Holocene	Qigequan Fm	7
1.8	Pleistocene		
	Pliocene	Shizigou Fm	6
5.3			
7.3	Miocene (Messinian)		
	Miocene (Tortonian-Langhian)	Shangyoushashan Fm	5
15.8			
	Lower Miocene	Xiayoushashan Fm	4
	Oligocene (Chattian)		
24.5			
	Oligocene (Chattian-Rupelian)	Shangganchaigou Fm	3
33.7			
	Eocene (Priabon)		
37.0			
40.3	Eocene (Bartonian-Ypresian)	Xiaganchaigou Fm	2
51.5			
	Eocene (Ypresian)	Lulehe Fm	1

Figure 2: Lithostratigraphy of the Qaidam basin (from Rieser et al., 2009).

levels with evaporate deposition ages at 302 ± 56 ka, 138 ± 6 ka, and 16.3 ± 2.2 ka.

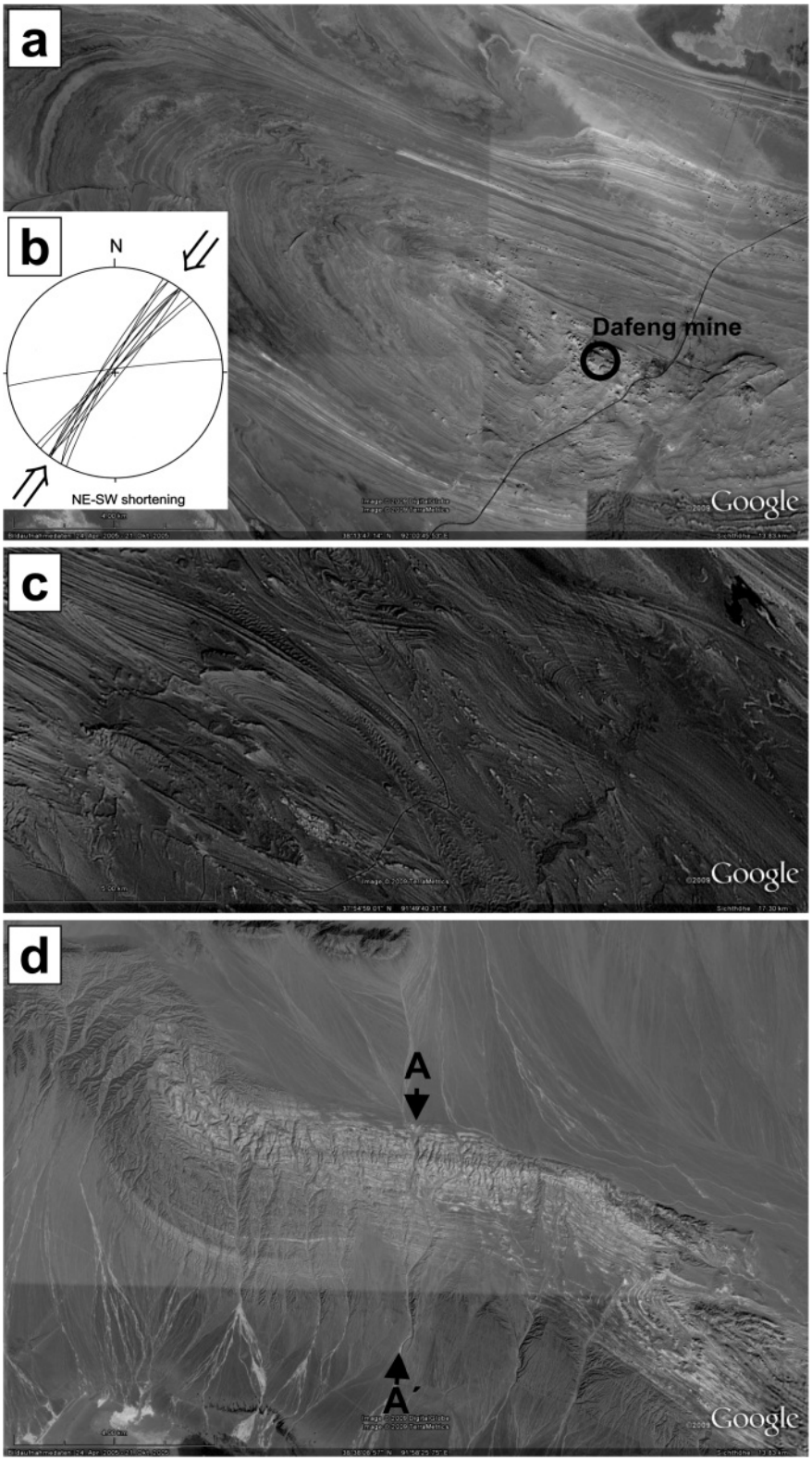

Figure 3: a - Satellite image of the Dafengshan. Note individual beds tracing the fold and abandoned Dafengshan celestine mine. The length/width ratio of the fold is ca. 4 : 1. b – Schmidt net with traces of discordant celestine veins at the abandoned Dafengshan celestine mine. c, d - Satellite image of the southern Youshashan (c) and Hongsanhan (d) anticlines. Note traces of individual beds. At Hongsanhan, the fold is northwards overturned. A–A´shows section in Figure 6e. For locations of images a, c, d, see Fig. 1. Satellite images a, c and d are from www.google.com.

The distribution of the present-day evaporates is well investigated and includes several facies (Lowenstein et al., 1989). These include three major evaporate facies: Na-Cl solutes, sulphate brines, and Na-Mg-Cl solutes (e.g., Casas et al., 1992; Vengosh et al., 1995; Warren, 1997, 2010 for a review).

Folding resulted in ca. ESE-trending anticlines (Fig. 1), which dominate the western Qaidam basin and which are easily recognizable. Along the northern basin margins thrust faults and strike-slip faults have been observed (Song and Wang, 1993; Métivier et al., 1998; Yin et al., 2008 and references therein). Crustal-scale folding of the Qaidam basin fill has been reported by Meyer et al. (1998), Zhou et al. (2006), and Meng and Fang (2008). GPS-data indicate ongoing NE-SW oriented shortening across the Qaidam basin and also some accommodation of convergence along the sinistral Kunlun and Altyn strike-slip faults (Bendick et al., 2000; Wang et al., 2001), which also resulted in squeezing the western Qaidam basin and eastward lateral extrusion of the Qaidam block in between. Global positioning data indicate NE motion of the Qaidam block in respect to stable Eurasia (Hilley et al., 2009 and references therein).

Measurements in drillholes in the western Qaidam basin have revealed a relatively high geothermal gradient (26.5 °C/km), in the northern part a significantly lower one (20.7 °C/km (Qiu, 2002).

3. Dafengshan anticline and celestine veins at Dafeng

The Dafengshan structure is a gentle dome-like WNW-trending anticline in the western central Qaidam basin, which is easily recognizable in satellite images (Fig. 3a). The core of the anticline exposes subhorizontal mudstones and rare marls and limestones of the Pleistocene Qigequan Formation interpreted as lake center facies. The succession is currently being eroded and is exposed in a

relictic yadan-type landform. At the abandoned Dafengshan celestine mine (Fig. 2), celestine forms several decimeter thick layers overlying marl and rare limestones, which are partly rich in bivalve shells. Celestine was precipitated as diagenetic cement within limestones, too (Fig. 4e; for details, see Bojar et al., 2005). Post-depositional mobilization of celestine resulted in formation of epigenetic subvertical, NNE-trending, ca. 1 – 3 decimeter thick extensional veins, which are filled with celestine (Fig. 4a–c). These celestine veins strike NNE–SSW (Fig. 3b) and therefore formed during regional SSW-NNE compres-

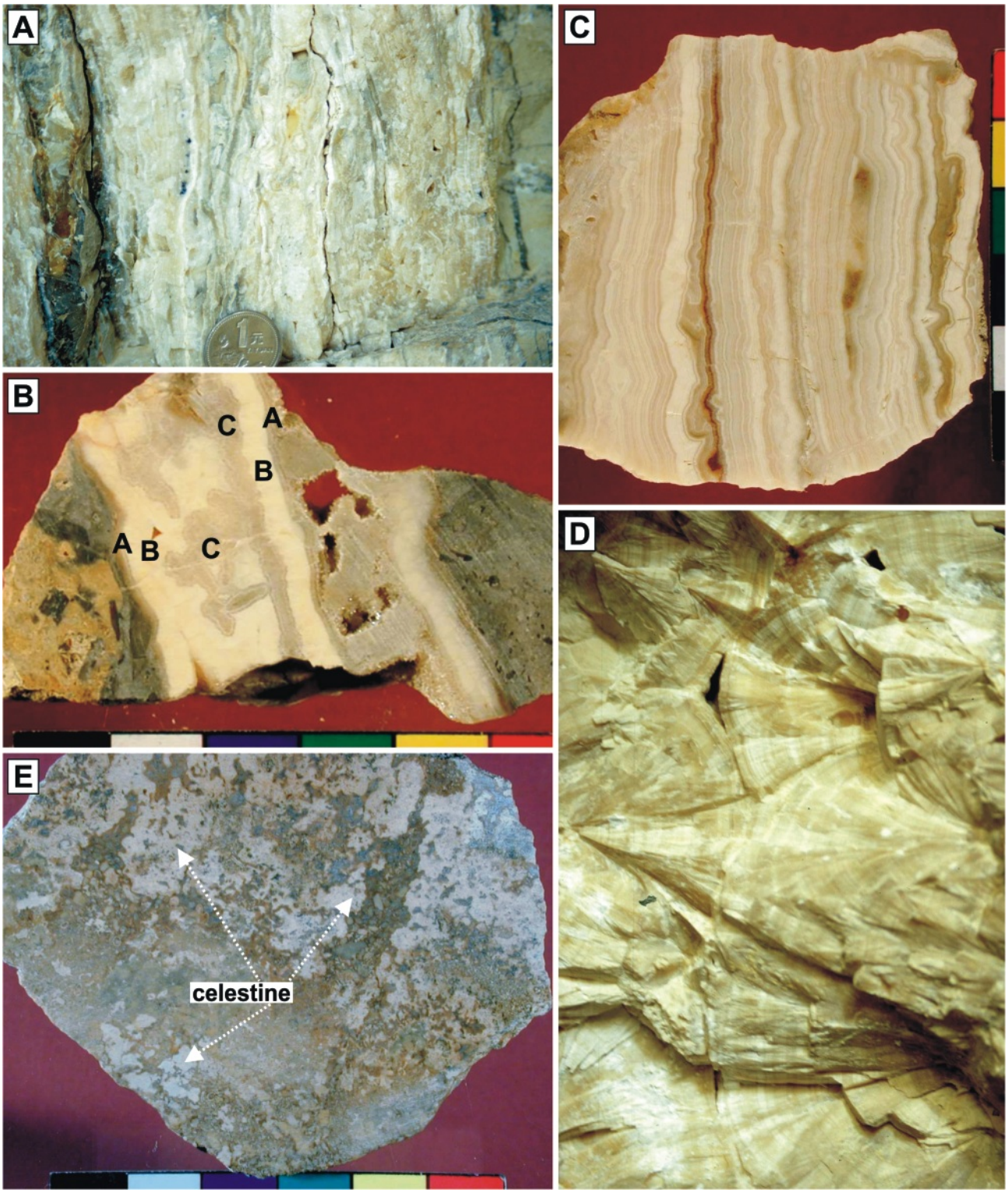

Figure 4: Field photographs of the structures and textures of celestine in the Dafengshan deposit. a – Vein with multiple near symmtrical infill. b – Three generations of celestine. For description, see text. c – Asymmetrical infill in a celstine vein, with reddish clays in the center. d - Regular radial growth of fibrous celestine crystals in a vein filled by framboid-like veins. e – Limestone is irregularly cemented by celestine (white). Division of scale bar in B, C, and E: 1 cm. short edge of picture in D: ca. 6 cm.

al., 2005). Post-depositional mobilization of celestine resulted in formation of epigenetic subvertical, NNE-trending, ca. 1 – 3 decimeter thick extensional veins, which are filled with celestine (Fig. 4a–c). These celestine veins strike NNE–SSW (Fig. 3b) and therefore formed during regional SSW-NNE compression, perpendicular to the strike of the Dafengshan anticline and consistent with other basin-scale structures like folds (Fig. 1).

Locally, three generations of celestine could be distinguished by their color within a single vein (Fig. 4b). These include an initial grey celestine generation (A in Fig. 4b) followed by a stage with white celestine (B in Fig. 4b), again followed by grey and colorless celestine (C in Fig. 4b) filling some cavities. Energy-dispersive X-ray analyses (not shown) reveal a pure $SrSO_4$ composition, with no variations between celestine generations, and only insignificant traces of other elements, except Ba at location 3 in Fig. 5b. Other examples expose multiple repetitions of fibrous grey and white celestine in part in an asymmetrical succession (Figs. 4c, 5a). In other veins, celestine displays framboid-like fabrics with radial fibers of celestine (Fig. 4d). In thin sections epitaxial mineral grains grew perpendicularly to the vein walls (Figs. 5c, d) and fine-grained veinlets of celestine cross-cut older broad veins (Fig. 5d).

4. Gypsum veins in the Hongsanhan and southern Youshashan anticlines

We also investigated other anticlinal structures and report here data from two structures, namely the Hongsanhan and southern Youshashan anticlines. The southern Youshashan anticlinorium represents a well exposed sequence of WNW-trending anticlines and synclines with fold lengths of ca. 1 – 2 km (Fig. 3c). Bedding planes clearly demonstrate a great circle distribution in the Schmidt net, and fold limbs are partly steep (Fig. 6a). Both bedding parallel and discordant gypsum

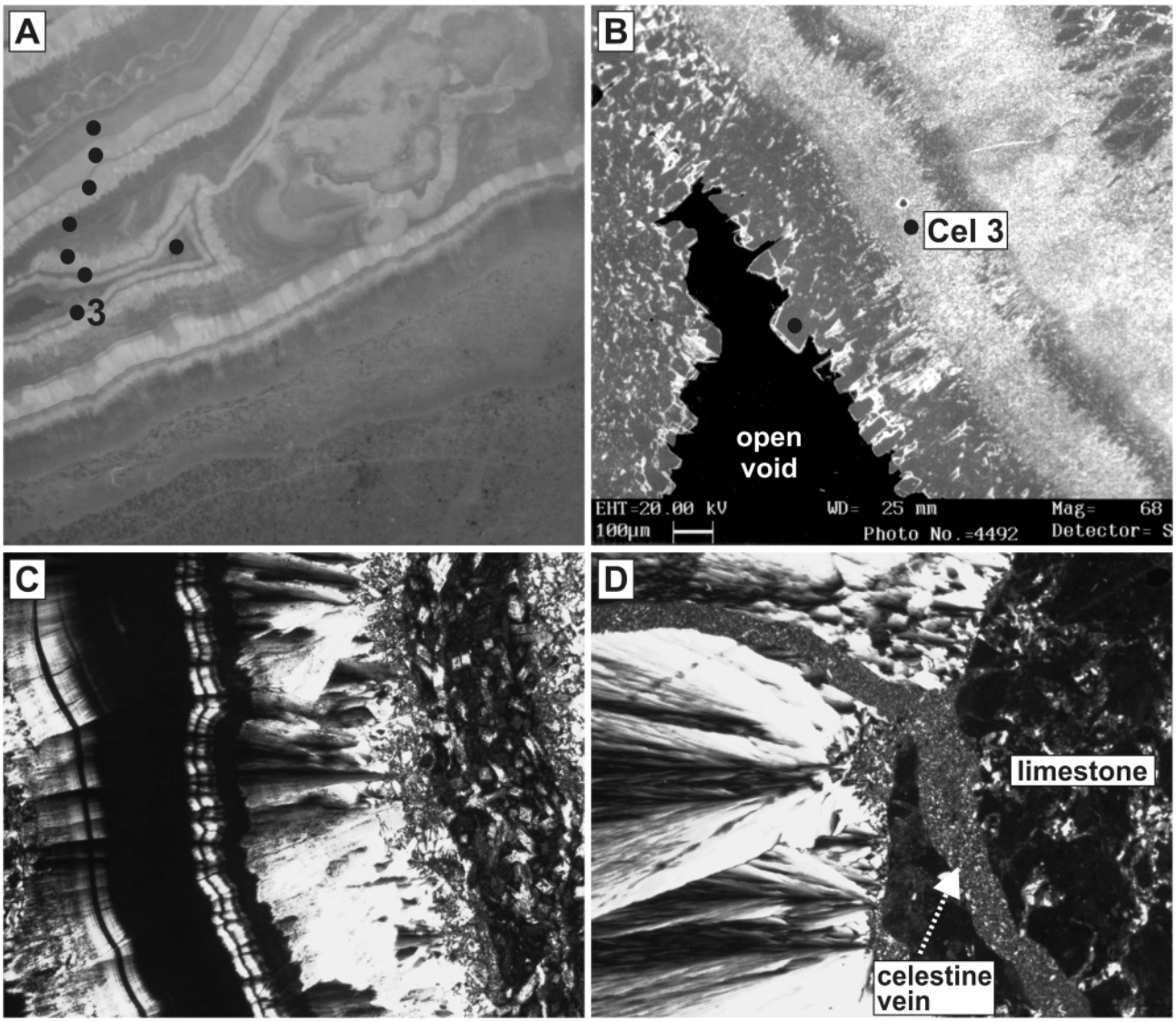

Figure 5: Microphotographs from celestine samples of Dafeng. a – Scanned thin section showing multiple generations of various celestine layers and open unfilled voids in the center. Long edge is ca. 4 cm. b – Scanning electron image showing open void in the center with euhedral small celestine crystals and a sequence of various celestine layers. c and d – Photomicrographs (crossed polarizers) of celestine layers showing multiple layers, epitaxial celestine growth, and a fine-grained celestine vein (only in d) cross-cutting earlier celestine fabrics. Long edge is ca. 4 mm.

veins are widespread in these folds. Bedding-parallel veins are ca. 3 cm thick, symmetrical and are composed of fibrous, epitaxial gypsum crystals. Discordant veins show a similar structure, and several generations of veins can be distinguished, overprinting each other. Discordant veins occur in two orientations, a dominant orientation perpendicular to the fold axis and striking in NNE-SSW direction, and a subordinate orientation parallel to the fold axis (Fig. 6b).

Formation	Lithostratigraphic formation and rock type	Coordinates	Sample no.	$^{87}Sr/^{86}Sr$	Error (2σ)
Pleistocene	Qigequan (Q_{1+2}), celestine	N 38°12.911´ E 92° 03.308´	QA-141D	0.711414	0.000005
			QA-141A	0.711418	0.000006
Miocene	Shangganchaigou (N_1), limestone	N 38° 24.089´ E 90° 53.132´	QA-92A	0.711578	0.000006
Oligocene	Xiaganchaigou (E_3), limestone	N 38° 26.289´ E 90° 52.316´	QA-88C	0.711679	0.000008

Table 1: Sr isotope composition of limestones (mainly Shizigou section) and celestine (Dafeng).

The Hongsanhan anticline is a ca. E-trending, northwards overturned anticline with a gently south-dipping fold limb exposing a stratigraphic section ranging from the Shangganchaigou to the Qigequan Formation (Figs. 3d, 6e). Details of the geology of the Hongsanhan anticline can be found in Rieser et al. (2010). Reverse and normal faults transect fold limbs. Bedding planes show again a great circle distribution in the Schmidt net (Fig. 6c). Bedding-parallel gypsum veins reach a thickness of 3 cm and are commonly symmetrically filled by fibrous epitaxial gypsum crystals (Fig. 7). Veins in this orientation dominate, whereas gypsum-filled discordant subvertical veins are subordinate and oriented roughly subperpendicular to the fold axis (Fig. 6d). They scatter widely in the Schmidt net.

5. Strontium isotopic composition

Strontium isotopic compositions of celestine from the abandoned Dafeng deposit as well as from Oligocene and Miocene limestones were measured on unspiked samples. The samples were analyzed at the Laboratory of Geochronology, University of Vienna. Details of the analytical procedure can be found in Tumiati et al. (2003). Within-run fractionation correction of Sr isotopes was normalized to $^{86}Sr/^{88}Sr = 0.1194$. The $^{87}Sr/^{86}Sr$ ratio for the NBS987 (Sr) standard was 0.710250 ± 0.000017 (n = 6) (Finnigan™ MAT262 mass spectrometer) and no correction was applied (Tumiati et al. 2003).

We selected limestone and celestine samples free from any visible admixture such as clay minerals. The celestine and limestone samples should represent a perfect mixture of various sources in the surrounding mountain belts due to the endorheic drainage.

The sample sites and analytical data are reported in Table 1. The Oligocene and Miocene limestone samples from the Shizigou section (see Fig. 1 for location) show $^{87}Sr/^{86}Sr$ ratios of 0.711578 ± 0.000006 and 0.711679 ± 0.000008, respectively. Samples of syn- and epigenetic celestine from the Pleistocene Dafeng deposit yielded values of 0.711414 ± 0.000005 and 0.711418 ± 0.000006, respectively, showing (1) an identical Sr isotope composition for these two texturally different types and (2) only slightly lower values than those from limestones.

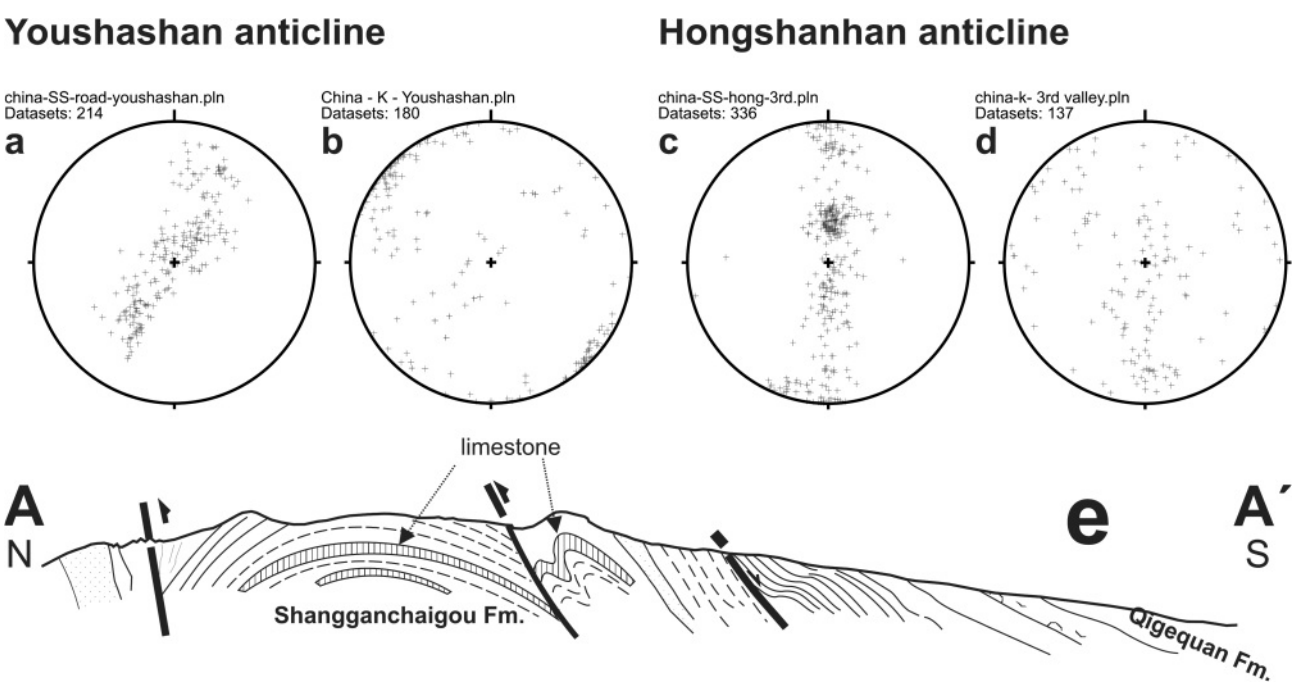

Figure 6: Orientation data (bedding and gypsum veins) of the southern Youshashan anticlinorium and the Hongsanhan anticline. a, b - Bedding planes; c, d - subconcordant and subvertical discordant gypsum veins. a – d, Lambert projection, lower hemisphere (vulgo Schmidt net). e – Section of the Hongsanhan anticline along Hongsanhan Third Valley. For location, see Fig. 3d.

We compare these data with available initial Sr isotopic ratios from various basement rocks from the wider catchment of the Qaidam basin including the Altyn, Qilian, and eastern Kunlun Mts. and also from the mountains surrounding the Hoh Xil (Kokoxili) basin to the west of the Qaidam basin. These data are compiled in Table 2 and are graphically shown in Fig. 8. The data show a large variation, but do not cover a wide range of rocks. In any case, significant changes in the isotopic compositions of the hinterland would have resulted in a significant change in the isotopic composition of the limestones and celestine, respectively.

Sr isotopic ratios from Qaidam evaporites are much higher than isotopic compositions of carbonates precipitated from Oligocene, Neogene and Pleistocene seawaters (DePaolo and Ingram, 1985) and reflect, therefore, the erosion of relatively old continental crust.

6. Discussion

6.1 Origin of celestine and gypsum veins

In the Qaidam basin, the annual average temperature is 2.7 °C, the daily maximum temperature reaches 34.2 °C (at Lenghu, see Fig. 1), the precipitation does not exceed 20 mm/yr, and the evaporation rate is 3096 mm/yr (Zhang and Xuan, 1996). In the Qaidam basin, the three main sources of water inflow are: surface river waters (mainly from the surrounding mountains which show higher precipitation than the basin), hot springs, and subsurface brines (Lowenstein et al., 1989; Vengosh et al., 1995; Liu et al., 2000, 2004). Meteoric precipitation is of minor importance in the basin because of the low precipitation in the basin itself. The hot springs/hydrothermal water is enriched in Na, $[SO_4]^{2-}$, and B. Surface river waters are of the Na-(Mg-Ca)-Cl type, and discharging subsurface brines are controlled by both salt dissolution and dolomitization processes and are rich in sulphate (Lowenstein et al., 1989; Ayora et al., 1994; Vengosh et al., 1995; Liu et al., 2000, 2004). Consequently, both the celestine and gypsum veins well reflect the composition of present-day subsurface brines. Gypsum is the dominant mineral species in more marginal anticlines, and celestine veins mainly occur in the Qaidam basin center. This may reflect the sequence of precipitation, where Ca was preferentially removed from brines by precipitation of first carbonates and then gypsum, and the remaining subsurface brine enriched in Sr. Consequently, the Sr veins at Dafeng reflect an advanced stage of enrichment in the center of the Qaidam basin.

The gypsum veins formed at a shallow thermal level, believed to be below ca. 42 °C in the presence of water at low confining pressure (Murray, 1964). At higher temperatures, gypsum is transformed to anhydrite. Rieser et al. (2005) noted the presence of anhydrite as the principal cement mineral in some sandstones collected from wells of the central Qaidam basin. In gypsum veins, no signs of transformation were observed and the original gypsum fibers are preserved within the investigated sections. The gypsum fibers precipitated at less than ca. 2 km overburden, assuming a geothermal gradient of 20.7 °C/km (Qiu, 2002).

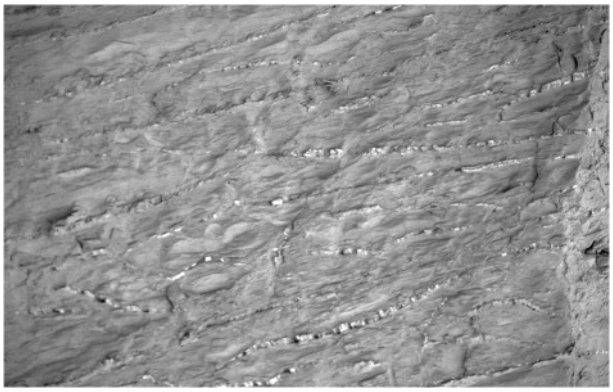

Figure 7: Gypsum veins subconcordant to bedding within marls exposed in the Hongsanhan Third Valley. Note symmetrical infill and gypsum fibers perpendicular to bedding. The veins are ca. 2.5 cm thick and comprise epitaxial fibers.

6.2 Kinematics deduced from veins

Tension gashes (or extensional veins) within folds with an orientation perpendicular to the fold axis are a common feature and have commonly been observed in many folds (e.g., Ramsay and Huber, 1983). They are well-known in the old terminology as filled ac-fractures. In dominant cases, these tension gashes are filled by quartz or calcite, and often also ore minerals precipitated from hydrothermal solutions. The orientation can be used as a paleostress marker. Commonly, the maximum principal stress as well as the shortening direction is parallel to the vein walls. Applied to the investigated cases, this means a ca. N-S shortening in the Hongsanhan, and NNE-SSW shortening in the southern Youshashan and Dafengshan anticlines, respectively. The age of formation is constrained by the age of the hosting formation, which is the Quaternary Qigequan Formation for Dafengshan. Consequently, the celestine veins record the orientation of Quaternary stress fields.

Geodetic data including GPS indicate ca. NE-SW shortening in the Qaidam basin area (Bendick et al., 2000; Wang et al., 2001; Hilley et al., 2009). This orientation is virtually different from NNE-SSW veins in the Dafengshan and southern Youshashan anticlines. Consequently, the GPS motion direction is different from the Late Quaternary shortening direction. This might reflect the increasing shortening and deflection of overall NNE motion of the Qaidam block into eastward extrusion and Qaidam-internal shortening.

6.3 Sr isotopic composition as a tracer of Qaidam basin fill

Our few Sr isotopic data of Oligocene and Miocene limestones and Pleistocene celestine show no significant variation through time and only represent a pilot study. For the interpretation of the Sr isotopic data, the Sr budget is important, and Sr is enriched in carbonates, evaporites, and mafic magmatic rocks. No evaporites and nearly no carbonates are ex-

posed in the surroundings of the Qaidam basin. The most abundant rocks are metapelitic and metapsammitic rocks and leucocratic granitoids, and some minor exposure of mafic metamagmatites. Unfortunately, only a few $^{87}Sr/^{86}Sr$ data were published from mountain ranges in the surroundings of the Qaidam basin (Table 2). The published data are from a wide variety of rocks. The initial $^{87}Sr/^{86}Sr$ ratio ranges from 0.70746 ± 0.00008 (Jingyu granite in the surroundings of the Hoh Xil (Kokoxili) basin in the west of the Qaidam basin; Roger et al., 2003) to 0.7312 ± 0.0006 (Xidatan orthogneiss from Eastern Kunlun Mts.; Arnaud et al., 2003). The Sr isotopic composition of the <75 µm grain size fraction of sediments from rivers draining the Kunlun Mts. was recently reported by Wu et al. (2010). They found $^{87}Sr/^{86}Sr$ ratios ranging from 0.719030 to 0.723426, i.e., much higher values than we found in celestine veins. The $^{87}Sr/^{86}Sr$ values of the <75 µm fraction of desert sands is more uniform and varies from 0.716605 to 0.719714, those of the <2 and the <75 µm fraction from other samples is significantly higher and between 0.726597 and 0.733062 (Chen et al., 2007). In spite of the variability of the values, the narrow band of Sr isotopic values in Oligocene to Pleistocene rocks from the Qaidam basin indicate that there was no major change in the composition through time. Because of the limited number of analyses, this interpretation must be taken with caution. The low variability of Sr isotopic compositions supports earlier observations of Rieser et al. (2005) that no significant change of the clastic composition occurred during the Eocene to Quaternary evolution of the Qaidam basin. The preliminary Sr isotope curve of the Qaidam basin is in contrast to the marine isotope curve, which exhibits much lower values and shows a regular increase of Sr isotopic values of ca. 0.7078 during late Eocene (at ca. 37 Ma before present) to a value of 0.7092 at the onset of the Holocene (DePaolo and Ingram 1985; Banner, 2004). The marine curve is interpreted to record the increase of erosion from Oligocene onwards during the Cenozoic Alpine-Himalayan orogeny. This contrasts with data from the Qaidam basin, where the Sr isotopic composition does not indicate a significant change through time.

Mountain range	Rock type	$(^{87}Sr/^{86}Sr)_{initial}$	Error (2σ)	Reference
Kokoxili	Wei Xue Shan granite	0.7069	0.0002	Roger et al. (2003)
Kokoxili	Jingyu granite	0.70746	0.00008	Roger et al. (2003)
Altyn Shan	Silicate marble	0.7126	0.0002	Delville et al. (2001)
North Altyn Shan	Bashikaogong porphyric granite	0.71758	not given	Wu et al. (2009)
North Altyn Shan	Dapinggou, quartz veins	0.71006	0.00018	Chen et al. (2004)
Eastern Kunlun	Xidatan orthogneiss	0.7312	0.0006	Arnaud et al. (2003)
Eastern Kunlun	deformed pegmatite	0.7138	0.0001	Arnaud et al. (2003)

Table 2: Previously published initial $^{87}Sr/^{86}Sr$ ratios from various rocks from mountains surrounding the Qaidam basin.

7. Conclusions

Our new data allow the following major conclusions:

1) Shortening also resulted in fluid flow and precipitation of sulphates in subvertical tension gashes, particularly of celestine and fibrous gypsum.
2) The orientation of these subvertical veins is similar over large portions of the western Qaidam basin and indicates NNE-SSW shortening significantly different from the present-day motion direction deduced from geodetic (GPS) data.
3) In deeper stratigraphic levels of anticlinal cores, tension gashes composed of fibrous gypsum subparallel to bedding demonstrate fluid overpressure during its formation below the conversion temperature of gypsum to anhydrite. We interpret these veins as near-surface precipitates from sulphate-dominated fluids during an advanced stage of folding.
4) The $^{87}Sr/^{86}Sr$ ratio of Quaternary celestine veins at Dafeng is 0.711414 ± 0.000005 and 0.711418 ± 0.000006 and is similar to that from Oligocene and Miocene limestones (0.711578 ± 0.000006 to 0.711679 ± 0.000008), thus monitoring only minor changes - although the data base is sparse - in the average $^{87}Sr/^{86}Sr$ composition from Oligocene to Quaternary despite highly heterogeneous source areas.

Acknowledgements

We gratefully acknowledge detailed reviews and suggestions by Christoph Spötl, an anonymous reviewer and by the

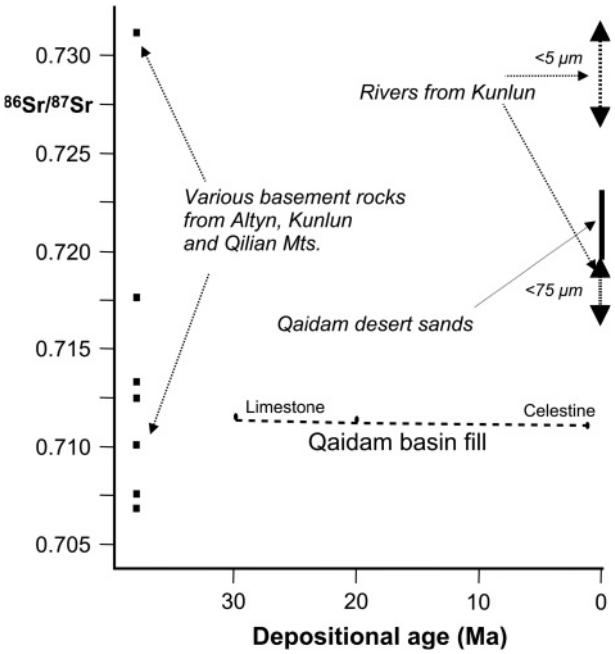

Figure 8: Sr isotopic evolution from Oligocene to Quaternary in the Qaidam basin fill. For comparison initial $^{87}Sr/^{86}Sr$ isotopic ratios from various basement rocks and river sediments from Kunlun are plotted. For data sources, see Table 2 and Chen et al. (2007) and Wu et al. (2009).

editor, Martin Zuschin. YL acknowledges support through project 4097248-NSFC of the National Science Foundation of China. Field work has been supported by the Qinghai Oil Company. Monika Horschinegg is thanked for performing the Sr isotope analytical work.

References

Arnaud, N., Tapponnier, P., Roger, F., Brunel, M., Schärer, U., Wen, C. and Xu, Z.Q., 2003. Evidence for Mesozoic shear along the western Kunlun and Altyn-Tagh fault, northern Tibet (China). Journal of Geophysical Research Solid Earth, 108, B1, article 2053.

Ayora, C., Garciaveigas, J. and Pueyo, J.J., 1994. The chemical and hydrological evolution of an ancient potash-forming evaporite basin as constrained by mineral sequence, fluid inclusion composition, and numerical simulation. Geochimica et Cosmochimica Acta, 58, 3379–3394.

Banner, J.L., 2004. Radiogenic isotopes: systematics and applications to earth surface processes and chemical stratigraphy. Earth-Science Reviews, 65, 141–194.

Bendick, R., Bilham, R., Freymueller, J., Larson, K. and Yin, G., 2000. Geodetic evidence for a low slip rate in the Altyn Tagh fault system. Nature, 404, 69–72.

Bojar, A.-V., Rieser, A., Neubauer, F., Bojar, H.-P., Genser, J., Liu, Y. and Ge, X.-H., 2005. Stable isotope and mineralogical investigations of an arid Quaternary lacustrine paleoenvironment, Western Qaidam, China. Geological Quarterly, 49, 173–184.

Bons, P.D., 2000. The formation of veins and their microstructures. In: M.W. Jessell and J. L. Urai (eds.), Stress, Strain and Structure, a Volume in Honour of W.D. Means. Journal of the Virtual Explorer, 2, paper 4, doi:10.3809/jvirtex.2000.00007.

Bons, P. D., 2001. Development of crystal morphology during unitaxial growth in a progressively widening vein: I. The numerical model. Journal of Structural Geology, 23, 865–872.

Casas, E., Lowenstein, T. K., Spencer, R. J. and Zhang, P., 1992. Carnallite mineralization in the nonmarine, Qaidam Basin, China; evidence for the early diagenetic origin of potash evaporates. Journal of Sedimentary Petrology, 62, 881–898.

Chen, X.H., Wang, X.F., Gehrels, G., Yang, Y., Qin, H., Chen, Z.L., Yang, F., Chen, B.L. and Li, X.Z, 2004. Early Paleozoic magmatism and gold mineralization in the northern Altun, NW China. Acta Geologica Sinica - English Edition, 78, 515–523.

Chen, J., Li, G., Yang, J., Rao, W., Lu, H., Balsam, W., Sun, Y. and Ji, J., 2007. Nd and Sr isotopic characteristics of Chinese deserts: Implications for the provenances of Asian dust. Geochimica et Cosmochimica Acta, 71, 3904–3914.

Craw, D. and Campbell, J. R., 2004. Tectonic and structural setting for active mesothermal gold vein systems, Southern Alps, New Zealand. Journal of Structural Geology, 26, 995–1005.

Delville, N., Arnaud, N., Montel, J.-M., Roger, F., Brunel, M., Tapponnier, P. and Sobel, E.R., 2001. Paleozoic in the Altun Shan massif area, eastern Qilian Shan, northeastern Tibet, China. In: M.S. Hendrix and A.M. Davis (eds.), Paleozoic and Mesozoic tectonic evolution of central and eastern Asia: From continental assembly to intracontinental deformation. Geological Society of America Memoir, 194, pp. 269–292.

DePaolo, D.J. and Ingram, B.L., 1985. High-resolution stratigraphy with strontium isotopes. Science, 227, 938–941.

Groshong, R.H., Jr., 1988. Low-temperature deformation mechanisms and their interpretation. Geological Society of America Bulletin, 100, 1329–1360.

Gudmundsson, A., Berg, S.S., Lyslo, K. B. and Skurtveit, E., 2001. Fracture networks and fluid transport in active fault zones. Journal of Structural Geology, 23, 343–353.

Hanor, J. S., 2000. Barite-celestine geochemistry and environments of formation. In: C. N. Alpers, J. L. Jambor and D. K. Nordstrom (eds.), Sulfate Minerals, Crystallography, Geochemistry and Environmental Significance. Reviews of Mineralogy and Geochemistry, 40, pp. 193–275.

Hausegger, S., Kurz, W., Rabitsch, R., Kiechl, E. and Brosch, F.-J., 2009. Analysis of the internal structure of a carbonate damage zone: Implications for the mechanisms of fault breccia formation and fluid flow. Journal of Structural Geology, 14 p., doi:10.1016/j.jsg.2009.04.014.

Hilley, G. E., Johnson, K.M., Wang, M., Shen, Z.-K. and Bürgmann, R. 2009. Earthquake-cycle deformation and fault slip rates in northern Tibet. Geology, 37, 31–34.

Holland, M., Urai, J. L., 2009. Evolution of anastomosing crack–seal vein networks in limestones: insight from an exhumed high-pressure cell, Jabal Shams, Oman Mountains. Journal of Structural Geology, 12 p., doi:10.1016/j.jsg.2009.04.011.

Huang, Q., Huang, H. and Ma, Y., 1997. Geology of Qaidam basin and its Petroleum prediction. Beijing, Geological Publishing House, 158 pp.

Liu, WG, Xiao, Y. K., Peng, Z. C., An, Z. S. and He, X.X, 2000. Boron concentration and isotopic composition of halite from experiments and salt lakes in the Qaidam Basin. Geochimica et Cosmochimica Acta, 64(13), 2177–2183.

Liu, X., Cai, K. and Yu, S., 2004. Geochemical simulation of the formation of brine and salt minerals based on Pitzer model in Caka Salt Lake. Science in China Serie D Earth Sciences, 47(8), 720–726.

Lowenstein, T.K., Spencer, R.J. and Zhang, P., 1989. Origin of ancient potash evaporites: Clues from the modern nonmarine Qaidam Basin of Western China. Science, 245, 1090–1092.

Meng, Q.-R. and Fang, X., 2008. Cenozoic tectonic development of the Qaidam Basin in the northeastern Tibetan Plateau. Geological Society of America Special Paper, 444, 1–24.

Métivier, F., Gaudemer, Y., Tapponnier, P. and Meyer, B., 1998. Northeastward growth of the Tibet plateau deduced from balanced reconstruction of two depositional areas: The Qaidam and Hexi Corridor basins, China. Tectonics, 17, 823–842.

Meyer, B., Tapponnier, P., Bourjot, L., Métivier, F., Gaudemer, Y., Peltzer, G., Guo, S. and Chen, Z., 1998. Crustal thickening in Gansu-Qinghai, lithospheric mantle subduction, and oblique, strike-slip controlled growth of the Tibet plateau. Geophysical Journal International, 135, 1–47.

Murray, R. C., 1964. Origin and diagenesis of gypsum and anhydrite. Journal of Sedimentary Research, 34, 512–523.

Neubauer, F., Lips, A., Kouzmanov, K., Lexa, J. and Ivascanu, P., 2005. Subduction, slab detachment and mineralization: the Neogene in the Apuseni Mountains and eastern Carpathians. Ore Geology Reviews, 27, 13–44.

Philipp, S.L., 2008. Geometry and formation of gypsum veins in mudstones at Watchet, Somerset, SW England. Geological Magazine, 145, 831–844.

Philipps, F.M., Zreda, M.G., Ku, T.L., Luo, S., Huang, Q., Elmore, D., Kubik, P.W. and Sharma, P., 1993. Th-230/U-234 and Cl-36 dating of evaporate deposits from the western Qaidam basin, China – implications for glacial-period dust export from Central Asia. Geological Society of America Bulletin, 105, 1606–1616.

Qiu, N., 2002. Tectono-thermal evolution of the Qaidam Basin, China: evidence from Ro and apatite fission track data. Petroleum Geoscience, 8, 279–285.

Ramsay, J. and Huber, M., 1983. The techniques of modern Structural Geology. Volume 1: Strain analysis. Academic Press, London – New York, 307 pp.

Rieser, A. B., Neubauer, F., Liu, Y. and Ge, X., 2005. Sandstone provenance of north-western sectors of the intracontinental Cenozoic Qaidam basin, western China: tectonic vs. climatic control. Sedimentary Geology, 177, 1–18.

Rieser, A. B., Liu, Y., Genser, J., Neubauer, F., Handler, R., Friedl, G. and Ge, X.H., 2006. $^{40}Ar/^{39}Ar$ ages of detrital white mica constrain the Cenozoic development of the intracontinental Qaidam Basin, China. Geological Society of America Bulletin 118, 1522–1534, doi: GSB25962.

Rieser, A. B., Bojar, A.-V., Neubauer,, F., Genser, J., Friedl,,G., Liu, Y. and Ge, X., 2009. Monitoring Cenozoic climate evolution of northeastern Tibet: Preliminary results from the Qaidam basin, China. International Journal of Earth Sciences, 98, 1063–1075.

Rieser, A. B., Neubauer, F., Liu, Y. and Genser, J., 2010. Walking through geologic history across a Neogene, incised anticline of the northern margin of the Tibetan plateau: review and synthesis. Austrian Journal of Earth Sciences, 130, 29–41.

Roger, F., Arnaud, N., Gilder, S., Tapponnier, P., Jolivet, M., Brunel, M., Malavieille, J., Xu, Z.Q. and Yang, J.S., 2003. Geochronological and geochemical constraints on Mesozoic suturing in east central Tibet. Tectonics, 22, 4, 1037.

Schubel, K. A., Lowenstein, T. K., Spencer, R.J. and Zhang, P. X., 1991. Evaporite deposition in a shallow perennial lake, Qaidam basin, Western China. American Association of Petroleum Geologists Bulletin, 75, p. 668.

Sibson, R. H., 2001. Seismogenic framework for hydrothermal transport and ore deposition. In: J.P. Richards and Tosdal, R. M. (eds.), Structural Controls on Ore Genesis. Society of Economic Geologists Reviews, 14, pp. 25–50.

Sibson, R. H., 2003. Controls on maximum fluid overpressure defining conditions for mesozonal mineralization. Journal of Structural Geology, 26, 1127–1136.

Song, T. and Wang, X., 1993. Structural styles and stratigraphic patterns of syndepositional faults in a contractional setting: Examples from Quaidam Basin, northwestern China. American Association of Petroleum Geologists Bulletin, 77, 102–117.

Spencer. R. J., 2000. Sulfate minerals in evaporite deposits. In: C. N. Alpers, J. L. Jambor and D. K. Nordstrom (eds.), Sulfate Minerals, Crystallography, Geochemistry and Environmental Significance. Reviews of Mineralogy and Geochemistry, 40, pp. 173–192.

Sun, Z., Yang, Z., Pei, J., Ge, X., Wang, X., Yang, T., Li, W. and Yuan, S., 2005. Magnetostratigraphy of Paleogene sediments from northern Qaidam Basin, China: implications for tectonic uplift and block rotation in northern Tibetan plateau. Earth Planetary Science Letters, 237, 635–646.

Tan, H.B., Ma, H.Z., Mang, X.Y., Xu, J.X. and Xiao, Y.K., 2009. Fractionation of chlorine isotope in salt mineral sequences and application: Research on sedimentary stage of ancient salt rock deposit in Tarim Basin and western Qaidam Basin. Acta Petrologica Sinica, 25, 955–962.

Tumiati, S., Thöni, M., Nimis, P., Martin, S. and Mair, V., 2003. Mantle-crust interactions durin Variscan subduction in the Eastern Alps (Nonsberg-Ulten zone): geochronology and new petrological constraints. Earth and Planetary Science Letters, 210, 509-526.

Vengosh, A., Chivas, A.R., Starinskyb, A., Kolodnyb, Y. , Zhang, B. and Zhang, P., 1995. Chemical and boron isotope compositions of non-marine brines from the Qaidam Basin, Qinghai, China. Chemical Geology, 120, 135–154.

Wang, J., Wang, Y.J., Liu, Z.C., Li, J.Q. and Xi, P., 1999. Cenozoic environmental evolution of the Qaidam Basin and its implications for the uplift of the Tibetan Plateau and the drying of central Asia. Palaeogeography Palaeoclimatology Palaeoecolology, 152, 37–47.

Wang, Q., Zhang, P., Freymueller, J. F., Bilham, R., Larson, K. M., Lai, X., You, X., Nie, Z., Wu, J., Li, Y., Liu, J., Yang, Z. and Chen, Q., 2001. Present-day crustal deformation in China constrained by global positional system measurements. Science, 294, 574–578.

Warrak, M., 1996. Origin of the Hafit structure: implications for timing the Tertiary deformation in the Northern Oman Mountains. Journal of Structural Geology, 18, 803–818.

Warren, J.K., 1997. Evaporites, brines and base metals: Fluids, flow and 'the evaporite that was'. Australian Journal of Earth Sciences, 44, 149–183.

Warren, J.K., 2010. Evaporites through Time: Tectonic, climatic and eustatic controls in marine and nonmarine deposits. Earth Science Reviews, 98, 217-268.

Wu, C., Yang, J., Robinson, P.T., Wooden, J. SF., Mazdab, F.K., Gao, Y., Wu, S. and Chen, Q., 2009. Geochemistry, age and tectonic significance of granitic rocks in north Altun, northwest China. Lithos, 113, 423–436.

Wu, W., Xu, S., Yang, J., Yin, H., Lu, H. and Zhang, K., 2010. Isotopic characteristics of river sediments on the Tibetan Plateau. Chemical Geology, 269, 406–413.

Xia, W., Zhang, N., Yuan, X., Fan, L. and Zhang, B., 2001. Cenozoic Qaidam basin, China: A stronger tectonic inversed, extensional rifted basin. American Association of Petroleum Geologists Bulletin, 85, 715–736.

Yin, A., Dang, Y.-Q., Zhang, M., Chen, X.H. and McRivette, M.W., 2008. Cenozoic tectonic evolution of the Qaidam basin and its surrounding regions (Part 3): Structural geology, sedimentation, and regional tectonic reconstruction. Geological Society of America Bulletin, 120, 847–876.

Zhang, Y. and Xuan, Z., 1996. Economic evaluation of potassium and magnesium solid deposit in Kunteyi and Mahai Salt Lake of Qinghai Province. Journal of Salt Lake Science, 4(1), 36–45 (In Chinese with English abstract).

Zhou, J., Xu, F., Wang, T., Cao W. and Yin, C., 2006. Cenozoic deformation history of the Qaidam Basin, NW China: Results from cross-section restoration and implications for Qinghai–Tibet Plateau tectonics. Earth and Planetary Science Letters, 243, 195–210.

Received: 16 December 2009
Accepted: 12 July 2010

Franz NEUBAUER[1)*], Yongjiang LIU[2)], Johann GENSER[1)], Andrea Brigitte RIESER[1)3)], Gertrude FRIEDL[1)], Xiaohong GE[2)] & Martin THÖNI[4)]

[1)] Dept. Geography and Geology, University of Salzburg, Hellbrunnerstr. 34, A-5020 Salzburg, Austria;

[2)] Faculty of Earth Sciences, Jilin University, 130061 Changchun, China;

[3)] present address: Nagra, Hardstrasse 73, 5430 Wettingen, Switzerland;

[4)] Dept. of Lithospheric Research, Vienna University, Althanstr. 14, A-1090 Vienna, Austria;

[*)] Corresponding author, franz.neubauer@sbg.ac.at